ASTRONOMY & ASTROPHYSICS
SUPPLEMENT SERIES

AUGUST **1996**, PAGE 243

Astron. Astrophys. Suppl. Ser. **118,** 243-262 (1996)

Optical observations of planetary nebula candidates from the northern hemisphere⋆

G.C. Van de Steene[1,3,⋆⋆], G.H. Jacoby[2] and S.R. Pottasch[3]

[1] European Southern Observatory, Casilla 19001, Santiago 19, Chile
[2] NOAO , P.O. Box 26732, Tucson, AZ 35726, U.S.A.
[3] Kapteyn Astronomical Institute, P.O.Box 800, NL-9700 AV Groningen, The Netherlands

Received May 17, 1995; accepted January 8, 1996

Abstract. — We present Hα+[N II] images of 17 and low resolution spectra of 14 IRAS-selected planetary nebula candidates. The Hα+[N II] images are presented as finding charts. Contour plots are shown for the resolved planetary nebulae. From these images accurate optical positions and mean optical angular diameters were determined. Optical spectra show that the IRAS-selected and radio detected planetary nebula candidates are indeed planetary nebulae. Three planetary nebula candidates, previously not detected in the radio continuum were seen in Hα. They are larger, low surface brightness planetary nebulae. Most of these IRAS planetary nebulae are heavily extinct, having an average A_V of 7 magnitudes. About half of the planetary nebulae seem to be of low excitation, having central stars with an effective temperature probably $\sim$60.000 K or less.

Key words: planetary nebulae: general

1. Introduction

This is a continuation of the project to identify new Planetary Nebulae (PN) applying the method as proposed by Pottasch et al. (1988). Unidentified IRAS sources were selected from the IRAS Point Source Catalog (PSC) on the basis of far IR colors, which are typical of PN. Having selected the candidates, there are two steps in proving that they are PN: the first is to observe these objects in the radio continuum, and the second is to take optical spectra. Radio measurements are especially suitable for a first confirmation, because in this wavelength range the radiation is not attenuated by extinction. Additionally, the detection of radio continuum emission shows the presence of ionized gas, which is strong evidence that the object is a PN. Finally, with radio synthesis observations one can obtain accurate positions to verify a correct association and which are useful for optical identification. This was successfully done for PN candidates inside the galactic bulge (Pottasch et al. 1988; Ratag et al. 1990; Ratag & Pottasch 1991) and outside the galactic bulge (Van de Steene & Pottasch 1993, 1995). Second, to confirm that these IRAS-selected and radio detected PN candidates are indeed PN, they should be observed in the optical.
In this paper we present optical images of 17 and spectroscopy of 14 PN candidates, observable from the northern hemisphere (Van de Steene & Pottasch 1995; hereafter Paper I).

2. Selection of the planetary nebula candidates

The sample candidates were selected from the IRAS PSC on the basis of their colors that are typical of PN. Only IRAS sources falling within the color box $F12/F25 \leq 0.35$ and $F25/F60 \geq 0.35$ were chosen, to avoid confusion with galaxies and HII regions, having colors just outside this box ($F12$, $F25$, and $F60$ refer to the flux in the IRAS wavelength bands centered at 12, 25 and 60 μm respectively). About half the sample sources have good flux values (quality 2 or 3) at 12, 25, and 60 μm and the other half have an upper-limit at 12 μm, but very good quality (3) flux values at 25 and 60 μm. The PN candidates are further than 15 degrees in longitude from the galactic center, presumably outside the galactic bulge The list of these IRAS-selected and radio observed PN candidates was presented in Paper I.

Send offprint requests to: G.C. Van de Steene[1]
⋆Based on data acquired at Kitt Peak National Observatory
⋆⋆Visiting Astronomer at Kitt Peak National Observatory, National Optical Observatories, which is operated by the Association of Universities for Research in Astronomy, Inc., under cooperatieve agreement with the National Science Foundation

3. Observations

3.1. *Imaging*

Images of all IRAS-selected PN candidates were taken through an Hα+[N II] filter with the KPNO 0.9 m and 4 m telescopes at Kitt Peak National Observatory (KPNO), USA, during 1992 and 1993. The main goal of taking the Hα images was to identify the PN candidates, then to obtain accurate optical positions and use the images as finding charts for optical spectroscopy. We also wanted to determine the mean optical angular diameters of the PN, in order to compare them with those obtained from the radio continuum images.

Table 1. Imaging observing log of detected PN candidates

Object	Observers	Date	Tel.	Time
1818–0833	Jacoby/Ciardullo	05/04/92	4 m	120 s
1823–1047	Jacoby/McMillan	19/04/93	4 m	300 s
1824–1410	Jacoby/Ciardullo	05/04/92	4 m	120 s
1825–0940	Jacoby/Ciardullo	05/04/92	4 m	120 s
1827–0729	Jacoby/McMillan	19/04/93	4 m	300 s
1839–1418	Jacoby/McMillan	19/04/93	4 m	200 s
1840–1109	Jacoby/Ciardullo	06/04/92	4 m	120 s
1841+0343	VdSteene/Jacoby	24/05/92	0.9 m	600 s
1858+0821	Jacoby/McMillan	19/04/93	4 m	200 s
1859+1013	Jacoby/Ciardullo	06/04/92	4 m	120 s
1904+1038	VdSteene/Jacoby	11/06/93	0.9 m	600 s
1908+0422	VdSteene/Jacoby	11/06/93	0.9 m	600 s
1909+1326	VdSteene/Jacoby	25/05/92	0.9 m	600 s
1911+1534	VdSteene/Jacoby	25/05/92	0.9 m	600 s
1920+1122	VdSteene/Jacoby	11/06/93	0.9 m	600 s
1933–0400	VdSteene/Jacoby	14/06/93	0.9 m	60 s
1943+2251	VdSteene/Jacoby	11/06/93	0.9 m	600 s

Some images were taken with the KPNO 0.9 m telescope using the T2KA CCD during May 1992 and June 1993. The PN candidates were observed through the Hα+[N II] filter KPNO-1276 with a FWHM of 35 Å centered at 6565 Å and in the continuum through the KPNO-1376 filter with a FWHM of 271 Å centered at 6098 Å. The pixel size of the images taken with the KPNO 0.9 m telescope is $0\farcs68$ per pixel.

Some images were taken with the KPNO 4 m telescope using the T1KA CCD in 1992 and the T2KB CCD in 1993. The PN candidates were observed through the Hα+[N II] filter KPNO-1390 with a FWHM of 72 Å centered at 6587 Å. The continuum images were taken through the Harris R filter. The pixel size of the images taken with KPNO 4 m telescope is $0\farcs47$ per pixel.

The images were reduced using standard procedures in the IRAF reduction package as described by Massey (1992). Afterwards the images were searched for the presence of a PN near the center of the field using the following procedure: each Hα+[N II] image was divided by the continuum one, and all three images were blinked.

Table 1 gives the observation log for the Hα images in which a PN was identified. The first column indicates the PN, the second column the observer, the third column the observing date, the fourth column the telescope used and the fifth the exposure time of the images.

3.2. *Spectroscopy*

The Hα images were used as finding charts for spectroscopy. Spectra were taken at the KPNO 2.1 m telescope with Goldcam in July 1993. The slit aperture was $2\farcs5$, the length was $2\farcm5$ and the orientation east-west. The spectral range is from 3,600 Å to 7,400 Å and the spectral resolution is ~ 8 Å.

We first positioned a bright, nearby HST guide star in the slit and then offset the telescope to the accurately determined optical position of the PN. We used this offset process because these PN generally are not visible on an acquisition TV. Using the image we ascertained that we had the right object in the slit. The weather was not photometric. Due to cirrus we lost a variable amount of photons, even when the guide star remained visible. Sometimes the exposure had to be stopped. The PN candidate, the date and the actual exposure time are listed in Table 2.

Table 2. Spectroscopy observing log

Object	Date	Time
1818–0833	17/07/93	30 min
1823–1047	20/07/93	30 min
1824–1410	19/07/93	30 min
1825–0940	19/07/93	45 min
1827–0729	18/07/93	30 min
1839–1418	18/07/93	25 min
1840–1109	17/07/93	10 min
1841+0343	18/07/93	30 min
1858+0821	17/07/93	15 min
1859+1013	17/07/93	15 min
1908+0422	16/07/93	54 min
1909+1326	18/07/93	45 min
1911+1534	19/07/93	45 min
1920+1122	20/07/93	45 min
1933–0400	19/07/93	30 min
1943+2251	18/07/93	45 min

The spectra were reduced using standard procedures in IRAF, as described by Massey et al. (1992). The wavelength calibration was done using a HeNeAr calibration lamp. For deriving the response curve of the detector, 3 to 4 standard stars were observed each night, except for the first night, when the weather was so bad that we only observed one standard star.

Table 3. Comparison between radio and optical positions. All positions are given in 1950.0 coordinates

Object	l	b	RA IRAS	DEC IRAS	RA Radio	DEC Radio	RA Optical	DEC Optical
	°	°	h m s	° ′ ″	h m s	° ′ ″	h m s	° ′ ″
1818–0833	21.9	2.7	18 18 36.8	-08 33 12	18 18 37.3	-08 33 09	—	—
1823–1047	20.4	0.6	18 23 11.8	-10 47 15	18 23 11.6	-10 47 16	18 23 11.8	-10 47 15
1824–1410	17.6	-1.2	18 24 21.3	-14 10 36	18 24 22.8	-14 10 27	18 24 22.8	-14 10 29
1825–0940	21.6	0.8	18 25 01.1	-09 40 08	18 25 00.6	-09 40 09	18 25 00.7	-09 40 07
1827–0729[i]	23.9	1.2	18 27 48.9	-07 29 45	18 27 47.9	-07 29 45	18 27 48.0	-07 29 45
1840–1109[ii]	22.0	-3.1	18 40 10.4	-11 09 56	18 40 10.3	-11 09 56	—	—
1858+0821	41.5	1.7	18 58 41.5	08 21 16	18 58 41.5	08 21 20	18 58 41.6	08 21 17
1904+1038	44.1	1.5	19 04 10.7	10 38 41	19 04 10.4	10 38 41	19 04 10.6	10 38 41
1908+0422	39.1	-2.2	19 08 24.1	04 22 26	19 08 24.4	04 22 28	19 08 24.5	04 22 28
1909+1326	47.2	1.8	19 09 17.6	13 26 06	19 09 17.3	13 26 09	19 09 17.4	13 26 08
1911+1534	49.3	2.4	19 11 02.9	15 34 27	19 11 03.1	15 34 31	19 11 03.2	15 34 30
1920+1122	46.7	-1.6	19 20 29.0	11 22 03	19 20 29.1	11 22 09	19 20 29.3	11 22 06
1933–0400	34.5	-11.7	19 33 39.5	-04 00 08	19 33 39.5	-04 00 00	19 33 39.6	-04 00 08
1943+2251	59.4	-0.7	19 43 26.1	22 51 11	19 43 25.8	22 51 12	19 43 25.9	22 51 12
1839–1418	19.2	-4.5	18 39 33.9	-14 18 11	18 39 34.4	-14 18 10	—	
1841+0343	35.4	3.5	18 41 07.0	03 43 35	18 41 07.2	03 43 37.1	—	
18599+1013[iii]	43.3	2.2	18 59 56.1	10 13 08	18 59 56.1	10 13 12	—	

[i] PN G 23.9+1.2 (Maehara 1992)
[ii] PN G 22.0−3.1 (Minkowski 1946)
[iii] PN G 43.3+2.2 (Capellaro et al. 1990)

4. Discussion

4.1. *Imaging*

The images of all identified PN candidates are presented in Appendix A, as finding charts. If the PN was resolved, its contour plot is shown as well in Appendix B.

Table 4. Comparison between radio and optical angular diameters. All angular sizes are given in arcseconds

Object	$\theta_{\rm PSF}$ Hα	$\theta_{\rm FWHM}$ Hα	$\theta_{\rm Str}$ Hα	$\theta_{\rm Str}$ 6 cm
1818–0833	1.5	1.7	3.1	6.8
1823–1047	2.1	2.5	4.5	6.6
1824–1410	1.7	ext.	11.2	17.8
1825–0940	2.3	2.5	4.5	3.6
1827–0729[i]	2.9	<2.9	<4.7	7.1
1840–1109[ii]	1.7	ext.	11.7	12.8
1858+0821	1.5	1.0	1.8	<13
1904+1038	2.0	3.2	5.8	6.4
1908+0422	1.6	ext.	10.7	<17
1909+1326	1.3	<1.3	<2.3	<3.1
1911+1534	1.4	<1.4	<2.4	<4.1
1920+1122	2.1	ext.	6.9	<8.2
1933–0400	1.8	0.8	1.4	<5.7
1943+2251	1.4	2.2	4.0	<7.7
1839–1418	1.9	ext.	17.5	–
1841+0343	1.6	ext.	4.5×13.8	–
1859+1013	2.0	ext.	17.9	–

4.1.1. Positional accuracy

The accurate optical position of the PN was obtained using the HST guide star catalog and the package FINDER in IRAF. The PN, its galactic longitude and latitude, the radio position and the optical position in 1950.0 coordinates are listed in Table 3.
For almost all PN, the optical position is within 3″ of the radio position. The accuracy of the optical positions is similar to the positional uncertainty of the HST guide stars, and thus better than 1″ in right ascension (RA) and declination (DEC). The accuracy of the radio positions depends upon the beamsize and the signal-to-noise ratio. The RA, obtained from the radio measurement, is also expected to be better than 1″. The DEC, obtained from the radio measurements, also depends upon sin(DEC). Because our sample PN are at low declinations, the accuracy in DEC could be worse than 1″. Therefore the optical declination is generally expected to be the most accurate.

For PN 1818–0833 and 1840–1109 insufficient HST guide stars were present in the field imaged to obtain an optical position. For the PN 1839–1418, 1841+0343 and 1859+1013, detected in Hα but not in the radio, the IRAS position is given.

The optical declination of PN 1933–0400 is 8″ off in declination compared to the radio position, but exactly on the IRAS position. Because the uncertainty of the declination in the radio is estimated to be 8″ (± 5″), the optical declination is within the accuracy of the radio

position. Therefore the radio, optical and IRAS sources are considered associated.

The optical PN 1859+1013 is about ten times the maximum uncertainty in declination away from the radio position: RA = $18^h59^m55^s.4$ and DEC = $10°14'00''$. However the IRAS position is in perfect agreement with the optical position. Consequently, the radio source is probably not associated with the optical PN. Another indication is that, based on its Hβ flux, PN 1859+1013 would have a radio flux below 1 mJy per beam, which is much below our detection limit of $\sim$3 mJy/beam.

The optical position of PN 1841+0343 is in perfect agreement with the IRAS position. In the radio map centered on the IRAS position, two radio sources are present: one of 7.1 mJy at RA = $18^h41^m09''.7$ and DEC = $3°44'46''$ mJy, and one of 4.0 mJy at RA = $18^h41^m07^s.1$ and DEC = $3°44'42''$. The first one is definitely too far away to be associated with the IRAS position. The second one is about three times further off the IRAS source in declination than its positional uncertainty. We don't think that any of the radio sources is associated with the PN. This needs to be confirmed.

4.1.2. Angular diameters

Optical: The point-spread function is well approximated by a gaussian with a FWHM of $\theta_{\rm PSF}$, derived from the second moments of the profiles of field stars and given in Col. 2 of Table 4. We also determined in this way the FWHM of the PN itself, $\theta_{\rm PN}$, and then calculated its deconvolved FWHM according to $\theta_{\rm FWHM} = \sqrt{\theta^2_{\rm PN} - \theta^2_{\rm PSF}}$ (given in Col. 3 of Table 4). However a gaussian profile is a rather poor description of the intensity distribution of a PN. In the case of a partially resolved object the best approach is to calculate $\theta_{\rm FWHM}$ and then apply a correction factor based on an assumed intensity distribution to obtain the true Strömgren angular diameter of the PN (Panagia & Walmsley 1978; Bedding & Zijlstra 1994). The Strömgren angular diameters, $\theta_{\rm Str}$, (given in Cols. 4 and 5 of Table 4) were calculated assuming that the ratio of the inner radius to the Strömgren radius is equal to a half. From the resulting intenstity distribution we determined that $\theta_{\rm FWHM}$ should be multiplied with a correction factor of 1.8 to obtain the Strömgren radius (van Hoof 1996, in preparation).

The PN for which the gaussian diameter is stellar an upper limit is given. The angular sizes of the well resolved PN were measured in RA and DEC from the lowest contour in the plots presented in Appendix B. Then the geometric mean diameter was calculated and listed as $\theta_{\rm Str}$ in Table 4.

Radio: For comparison the radio diameters are given in Table 4. The radio angular diameters are likely to be overestimated, due to the very elongated beam compared to the small sizes of the PN, and the lack of *uv*-coverage. From Table 4 it is clear that most radio diameters are larger than the optical diameters, and that the difference is worse than for the PN observed with the Australian Compact Array (Van de Steene & Pottasch 1993).

4.1.3. Detection statistics

Table 5 gives an overview of the IRAS PN candidates which were observed in the radio continuum, those which were detected (det), and those which were observed (obs) in the optical.
The radio detected candidate 1903+0801 (Paper I) wasn't observed in the optical.
The following PN candidates were detected in the radio continuum but not in Hα: 1853+0549, 1917+1252, 1935+2302. If they are indeed PN, they are probably undetected because of extinction (Kistiakowsky & Helfland 1993). The region around PN 1853+0549 is clearly very obscured.
The only PN detected in Hα for which we didn't obtain a spectrum is 1904+1038. We obtained spectra of PN 1825–0940 and PN 1858+0821, but the signal-to-noise ratios were so low, that we can't confirm their PN nature.

Table 5. Overview: detections and non-detections

Object	S_{6cm}	Hα	Spectrum
1818–0833	det	det	det
1824–1410	det	det	det
1825–0940	det	det	too low S/N
1840–1109	det	det	det
1909+1326	det	det	det
1911+1534	det	det	det
1917+1252	det	not det	not obs
1823–1047	det	det	det
1827–0729	det	det	det
1853+0549	det	not det	not obs
1858+0821	det	det	too low S/N
1903+0801	det	not obs	not obs
1904+1038	det	det	not obs
1908+0422	det	det	det
1920+1122	det	det	det
1933–0400	det	det	det
1935+2302	det	not det	not obs
1943+2251	det	det	det
1839–1418	not det	det	det
1841+0343	not det	det	det
1859+1013	not det	det	det

We obtained Hα+[N II] images of all PN candidates from Paper I which have a RA larger than 18^h, thus also of the forty candidates which weren't detected in the radio continuum. The larger PN: 1839–1418, 1841+0343, and 1859+1013, were detected in the Hα images, but not in our radio continuum observations. Based on their observed Hβ fluxes PN 1839–1418, 1841+0343, and 1859+1013 would

have a radio flux below 1 mJy per beam, which is much below the detection limit of ∼3 mJy/beam.

4.2. *Spectroscopy*

The spectra of the PN candidates detected in Hα are shown in Appendix C. The Table with line-identifications and line-ratios normalized to Hβ, or [O III]λ5007, depending upon which one was available and best determined, are presented in Appendix D. The line-fluxes were corrected for interstellar extinction using the extinction law from Seaton (1979). This typical interstellar extinction law and the observed Hα/Hβ ratio, when compared to the recombination value of 2.85 (Aller 1984), gives a logarithmic extinction at Hβ:

Table 6. Values for logarithmic extinction, A_V (mag) = 2.1 c(Hβ) = 3.1 c(Hα)

Object	c(Hβ)	c(Hα)	A_V mag	Excitation Class
1818–0833	2.7		5.7	5.5
1823–1047	5.3		11.1	4.0
1824–1410	3.3		6.9	5.1
1825–0940	—	2.1	6.5	—
1827–0729	4.6		9.7	0.1
1839–1418	1.5		3.2	9.8
1840–1109	1.1		2.3	7.3
1841+0343	2.3		4.8	0.3
1858+0821	—	3.4	10.5	—
1859+1013	1.9		4.0	4.0
1908+0422	—	2.8	8.7	8.0
1909+1326	3.2		8.7	7.7
1911+1534	—	2.7	8.4	5.7
1920+1122	—	2.8	8.7	8.4
1933–0400	0.8		1.7	0.0
1943+2251	—	3.0	6.3	11.0

c(Hβ) = 3.096 log(Hα / (Hβ 2.85),
which corresponds to a visual extinction of A_V = 2.1 c(Hβ). For PN without detectable Hβ emission, we used the previous expression for c(Hβ), together with the equation by Pottasch (1984) based on the radio flux:
c(Hβ) = log(S_{6cm} / (3.67 Hβ),
to eliminate Hβ from the equations and to derive the logarithmic extinction value at Hα (i.e. c(Hα)), which corresponds to a visual extinction of A_V = 3.1 c(Hα). However this is a rough estimate, because for the larger nebulae, some flux will have been missed due to the 2″ slit width, while the radio flux is measured over the whole PN. Furthermore the weather wasn't photometric, so that standard stars and PN weren't observed under the same sky conditions. The values for extinction based on Hα and radio flux are therefore likely to be less accurate. The values for the logarithmic extinctions are presented in Table 6. The fact that no Hβ emission was seen, is in itself a clear indication for a high extinction with A_V larger than ∼8 mag. While the values for A_V of optically known PN are in the range 0.04 to 4.8 mag (Osterbrock 1989), we notice that for only 5 of these 16 IRAS PN, A_V is smaller than 4.8. These IRAS PN have an average A_V = 6.7 mag.

After correction for extinction, the excitation class of the PN was calculated according to Dopita & Meatheringham (1990). The excitation classes are given in Col. 5 of Table 6. The relation between excitation class and stellar effective temperature is rather analogous to the relation between stellar spectral type and effective temperature in the case of stars. An excitation class higher than 5 means that He II λ4686 could be observed in the spectrum and that the stellar temperature is higher ∼60,000 K. From Table 6 we see that about half the number of PN are of low excitation.

5. Notes on individual objects

We searched the literature using the Simbad database to collect published information about the individual PN. All PN candidates except PN 1824–1410 were listed in Preite-Martinez (1988) as possible new PN. Next we checked whether the IRAS sources had an association in the "Catalogue of galactic PN" (Acker et al. 1992).

1818 − 0833

PK 021+02.1 was listed as a suspected PN by MacConnel (1978) and associated with the IRAS source 18186–0833 by Iyengar (1987). Manchado et al. (1989) in an abstract in the Revista Mexicana, mentioned that from low resolution spectra they found the object to be a PN of low excitation, which seems to have a high helium abundance. The nebula has no He II λ4686 emission, indicative of a stellar temperature below ∼60,000 K.

1823 − 1047

If we compare the spectrum of this PN to the one above they seem quite similar, despite the much higher extinction of PN 1823–1047.

1824 − 1410

Some interstellar Hα emission of material further away from the brighter PN is visible in the image, and it is not clear whether it has been associated with the PN. If one forget about the foreground stars, the contour plot of this PN looks much like PN 1908+0422, only the center seems brighter.

1825 − 0940

The spectrum of this probable PN has a very low signal to noise and only Hα, [N II]λ 6548 & 6583, [Ar III]λ 7135 and [O II]λ 7323 & 7332 are observed. Their line strengths after correction for extinction to Hα=100 are 20, 67, 12.6 and 11 respectively.

Table 7. Comparison of the flux ratios to Hβ=100 between the Strasbourg-ESO catalogue of galactic PN and our values for PN 1827-0729

λ (Å)	Ident	Catalogue	Ours
4686	HeII		
4363	[OIII]		
5007	[OIII]		15
5876	HeI		61
6563	Hα	4133	7044
6584	[NII]	4016	6925
6717	[SII]	139	192
6731	[SII]	251	349

1827 − 0729

Kistiakowsky & Helfland (1993) associated the radio source detected in the VLA 20 cm imaging survey (Zoonematkermani et al. 1990; Helfland et al. 1992) with the IRAS source, having colors typical of a PN. They imaged the PN candidate in R-band, Hα and [S III]λ9069 and λ9532. They measured an angular diameter of $2\farcs5 \pm 0\farcs1$ at FWHM, which is similar to our FWHM. They didn't mention $\theta_{\rm PSF}$, but multiplying this FWHM with 1.8 would give an angular diameter of $\sim 4''$.
This object is listed in the Strasbourg-ESO catalogue of galactic PN (PNG 023.9+01.2, Acker et al. 1992; Maehara 1982), as a PN with stellar appearance, though the association with this IRAS source is not mentioned.

Our spectrum of this object shows no [O III]λ4959 but we may observe very weak [O III]λ5007 emission. The spectrum shows Hβ emission. This PN would be of low excitation with a stellar temperature probably around 30,000 K.

In Table 7 we compare our unreddened flux ratios to Hβ with those mentioned in the Strasbourg-ESO Catalogue of galactic PN. The differences are too large to be attributed to the uncertainties in our measurements. The ratio of Hα to [N II] and the ratio of the [S II] lines are exactly the same in both cases. Our Hα value is stronger compared to the [S II] lines, than in the catalogue. We clearly observe He I λ5876, while it is not mentioned in the catalogue. This PN is stellar so that most of the object was in the slit. Therefore the changes in the spectrum may be real, likely due to the evolution of the central source towards higher temperature. It would be worthwile to monitor this PN.

1839 − 1418

This PN has a similar morphology than PN 1859+1013, though it has a more pronounced bar like structure in its center.

The spectrum of PN 1839–1418 has a higher signal-to-noise ratio than the spectrum of PN 1859+1013. This PN also seems to have a higher excitation. It shows a strong He II line in its spectrum, but no He I emission lines were observed. The most remarkable aspect of both spectra is the absence of the [N II]λ6548 & 6583 lines, indicating a low nitrogen abundance.

1840 − 1109

The position of this PN is in perfect agreement with PNG 022.0–03.1 in the Catalogue of galactic PN (Acker et al. 1992), though in the catalogue the association with the IRAS source is not mentioned. Our radio flux of 36 mJy at 6 cm is in agreement with the 40 mJy at 2 cm measured by Milne & Aller (1982), but much lower than the 60 mJy measured by Calabretta (1982). The optical diameter mentioned in the catalogue is $6\farcs4$, which is smaller than our angular size of $11''$. It is a very bright PN and the spectrum is the richest we obtained.

Table 8. Comparison of the flux ratios to Hβ=100 between the Strasbourg-ESO catalogue of galactic PN and our values for PN 1840–1109

λ (Å)	Ident	Catalogue	Ours
4686	HeII	56	48
4363	[OIII]	10	9
5007	[OIII]	1435	1398
5876	HeI	21	21
6563	Hα	739	687
6584	[NII]	76	87
6717	[SII]	9	9
6731	[SII]	14	14

In Table 8 we compare our reddened flux ratios to Hβ to the ones published in the Strasbourg-ESO catalogue of galactic PN. Our values are generally less or equal than the ones published in the catalogue, though within the estimated 10% accuracy of our values, except for He II λ4686 and [N II]λ6584. The latter might be due to the deblending. In the Strasbourg-ESO catalogue the slit width was $4''$ while we used a $2''$ slit. The difference could also be due to different orientation of the slit across this extended nebula.

1841 + 0343

Lewis et al. (1987) looked for but didn't detect any OH maser emission in PN 1841+0343. The source is located in region VIII, close to region IV, in the IRAS color-color diagram (Van der Veen & Habing 1988).
The PN is clearly bipolar and it would be interesting to investigate its morphology further.

1858 + 0821

Only Hα and [N II]λ6548 & 6583 have been observed in this very low signal to noise spectrum. After correction for extinction the strength of the forbidden nitrogen lines relative to Hα=100 are 24.4 and 66.4 respectively.

1859 + 1013

Was identified as a new PN from the Palomar Observatory Sky Survey (POSS) plates by Capellaro et al. (1990). They mention an optical diameter of $14''$, in agreement with our measurement.

This PN has a similar morphology than PN 1839–1418. The spectrum of PN 1859+1013 has a lower signal-to-noise ratio than the spectrum of PN 1839–1418. PN 1859+1013 also seems to be of lower excitation: it shows He I lines, but not He II, though the latter may be caused by extinction. The most remarkable aspect of both spectra is the absence of the [N II]λ6548 & 6583 lines, indicating a low nitrogen abundance.

1908 + 0422

This spectrum was taken during the first and worst observing night. Only a few forbidden lines are clearly visible in the spectrum, confirming its PN nature. This is one of the larger, resolved PN of high excitation discovered, as can be deduced from its [O III] to Hα line ratio.

1909 + 1326

This definitely seems to be a high excitation PN. It shows some [Fe II], [Fe III], [Fe IV], [Fe VII] emission lines in its spectrum. One would expect iron to be depleted in grains in PN, though iron has been seen in high resolution spectra of other PN such as IC 2165 (Huyng 1994) and IC 4997 (Hyung et al. 1994). IC 2165 has a hot central star and appears to consist of zones of quite different density. IC 4997 has a variable (Hyung et al. 1994) or binary central star which is surrounded by a compact, dusty, presumably young nebula and is best fit by a thin, high density shell and a larger, lower density shell. The presence of forbidden iron emission lines probably originate in the higher density regions of these nebula. The dust temperature and dust to gas ratio is high for both nebula. In Paper I we found that PN 1909+1326 has a dust temperature of 141 K and a large IRE=11.

1911 + 1534

This PN was also observed by Garcia-Lario et al. (1990) in the J, H and K near IR bands ($J = 12.0 \pm 0.1$, $H = 10.6 \pm 0.4$, $K = 10.1 \pm 0.3$). Lewis et al. (1987) looked for but didn't detect OH maser emission. The IRAS source is still located in region IV of the IRAS color-color diagram as defined by Van der Veen & Habing (1988).

The line at λ=4483.6 Å could be a blend of Mg and Fe lines (Meinel et al. 1969).

1920 + 1122

This object doesn't seem to have a central peak, is very small and faint, however not much can be said from the image itself at this resolution.

The spectrum has low signal-to-noise, shows very weak [O III]λ5007 emission and some [Ar III]λ7139.

1933 − 0400

A low resolution and low signal to noise spectrum of this Hα emission line star was published by Downes & Keyes (1988). They did mention that superposed on a slightly red sloping continuum are low excitation forbidden lines of [O II]λ3727, [N II]λ6583, and [S II]λ6717,λ6730 commonly found in PN spectra. Because no [O III]λ4959 & 5007 emission is observed, but the spectrum shows Hβ, this PN is definitely of low excitation with a stellar temperature below 30,000 K. This apparently young PN has the lowest value for the extinction in our sample. We didn't see C IV λ4658, which Downes & Keyes (1988) suspected to be present, but we detected C III λ4648 and Na I λ4648 in absorption in our spectrum. The presence of He I absorption lines classify its central star as a B I spectral type.

The blue component superposed on the red continuum suggests that this object could be binary, maybe a symbiotic nebula. However the radio continuum emission argues in favor of the PN nature of this object. D-type symbiotic stars and novae also show an emission line spectrum and often have radio continuum emission above 10 mJy. However known symbiotic stars have bluer IRAS-colors than PN. We would never have selected them as PN candidates, because their IRAS flux at 12 μm is too high compared to the 25 μm flux value (Whitelock 1988). It will be worthwile to keep monitoring this object.

1943 + 2251

From the contour plot it is clear that this PN is more elongated than the three field stars around it. It would be interesting to image this PN at much higher resolution to investigate its morphology in more detail.

6. Conclusions

We presented Hα+[N II] images of 17 and low resolution spectra of 14 IRAS-selected planetary nebula candidates. Almost all PN candidates selected from the IRAS PSC based on their colors typical for PN and detected in the radio continuum, were confirmed as PN by optical spectroscopy. Most of these IRAS PN are heavily extinct having an average A_V of 7 mag. Large extinction may be the reason why some of the radio detected PN candidates have gone undetected in Hα. On the other hand, a few IRAS-selected PN candidates, which were below our detection limit in the radio, have been detected in Hα. About half of the PN seem to be of low excitation, having a stellar effective temperature lower than $\sim$60,000 K. Careful modeling has been done in order to consistently determine the physical parameters of the PN with good optical spectra. The modeling used to obtain a self-consistent model and the results obtained will be discussed in forthcoming papers (Van Hoof & Van de Steene 1996; Van de Steene & van Hoof 1996, in preparation; Van de Steene 1995)

Acknowledgements. G.C. Van de Steene acknowledges support from the Netherlands Foundation for Research in Astronomy (ASTRON) under grant number 782-372-035. This research has made use of the Simbad database, operated at CDS, Strasbourg, France. We thank P.A.M. van Hoof for critical reading of the manuscript.

References

Acker A., Marcout J., Ochsenbein F., Stenholm B., Tylenda R., 1992, Strasbourg-ESO Catalogue of Galactic Planetary Nebulae, ESO

Aller L.H., 1984, Physics of Thermal Gaseous Nebulae, Reidel, Dordrecht

Bedding T.R., Zijlstra A.A., 1994, A&A 283, 955

Calabretta M.R., 1982, MNRAS 199, 141

Capellaro E., Turatto M., Salvadori L., Sabbadin F., 1990, A&AS 86, 503

Dopita M.A., Meatheringham S.J., 1990, ApJ 357, 140

Downes R.A., Keyes C.D., 1988, AJ 96, 777

Garcia-Lario P., Manchado A., Pottasch S.R., Suso J., Olling R., 1990, A&AS 82, 497

Helfland D.J., Zoonematkermani S., Becker R.H., White R.L., 1992, ApJS 80, 211

Hyung S., 1994, ApJS 90, 119

Huyng S., Aller L.H., Feibelman W.A., 1994, ApJS 93, 465

Iyengar K.V.K., 1987, A&AS 68, 103

Kistiakowsky V., Helfland D.J., 1993, AJ 105, 2199

Lewis B.M., Eder J., Terzian Y., 1987, AJ 94, 1025

MacConnel D.J., 1978, A&AS 33, 219

Maehara H., 1982, Contributions from the Bosscha Observatory No. 71

Manchado A., Garcia Lario P., Pottasch S.R., 1989, Rev. Astron. Astrofis. 18, 184

Massey P., 1992, A User's Guide to CCD Reductions with IRAF, IRAF help package

Massey P., Valdes F., Barnes J., 1992, A User's Guide to Reducing Slit Spectra with IRAF, IRAF help package

Meinel A.B., Aveni A.F., Stockton M.W., 1969, Catalog of emission lines in astrophysical objects, University of Arizona

Milne D.K., Aller L.H., 1982, A&AS 50, 209

Osterbrock D.E., 1989, Astrophysics of Gaseous Nebulae and Active Galactic, Nuclei, University Science, California, Ch. 7

Panagia N., Walmsley C.M., 1978, A&A 70, 411

Pottasch S.R., 1984, Planetary Nebulae, Reidel, Dordrecht, p. 93

Pottasch S.R., Bignell C., Olling R., Zijlstra A.A., 1988, A&A 205, 248

Ratag M.A., Pottasch S.R., Zijlstra A.A., Menzies J., 1990, A&A 233, 181

Ratag M.A., Pottasch S.R., 1991, A&AS 91, 481

Preite-Martinez A., 1988, A&AS 76, 317

Seaton M.J., 1979, MNRAS 187, 17

Van de Steene G.C., 1995, PhD Thesis Groningen

Van de Steene G.C., Pottasch S.R., 1993, A&A 274, 895

Van de Steene G.C., Pottasch S.R., 1995, A&A 299, 238 (Paper I)

Van der Veen W.E.J.C., Habing H.J., 1988, A&A 194, 125

Whitelock P., The symbiotic phenomenon, 1987. In: Mikolajewska J., Friedjung M., Kenyon S.J., Viotti R. (eds.). Kluwer, Dordrecht

Zoonematkermani S., Helfland D.J., Becker R.H., White R.L., Perley R.A., 1990, ApJS 74, 181

A. Hα+[N II] images

In this appendix all Hα+[N II] images in which a PN was identified are presented as finding charts. The PN is indicated by a box. North is at the top and east is to the right. For images 1 to 7, 9 and 10, taken with the KPNO 4 m telescope, the field of view is $4' \times 4'$. For images 8 and 11 to 17, taken wih KPNO 0.9 m telescope the field of view is $3' \times 3'$.

Fig. 1. 1818-0833

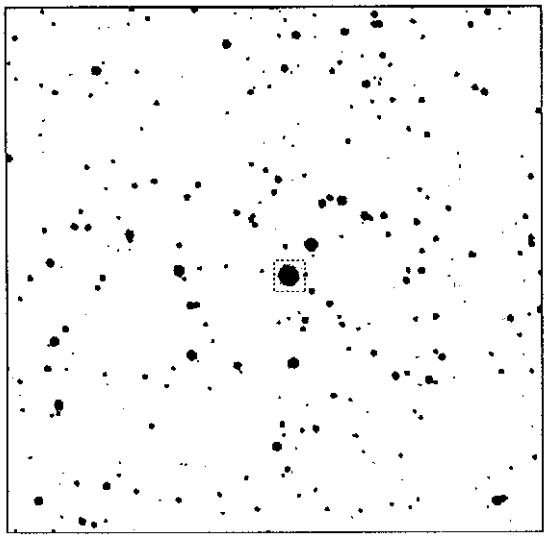

Fig. 2. 1823-1047

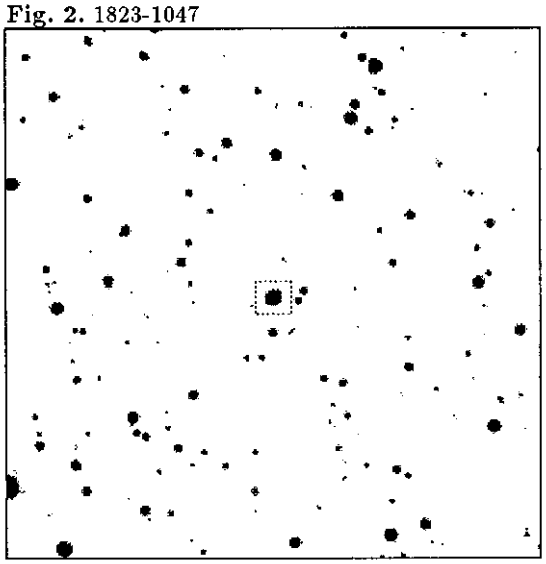

Fig. 3. 1824-1410

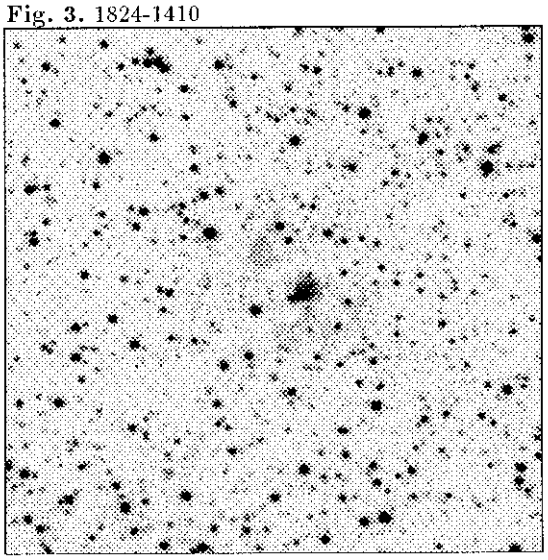

Fig. 4. 1825-0940

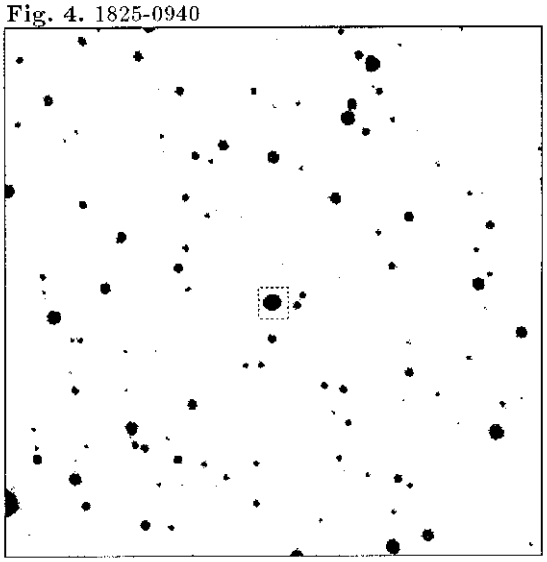

Fig. 5. 1827-0729

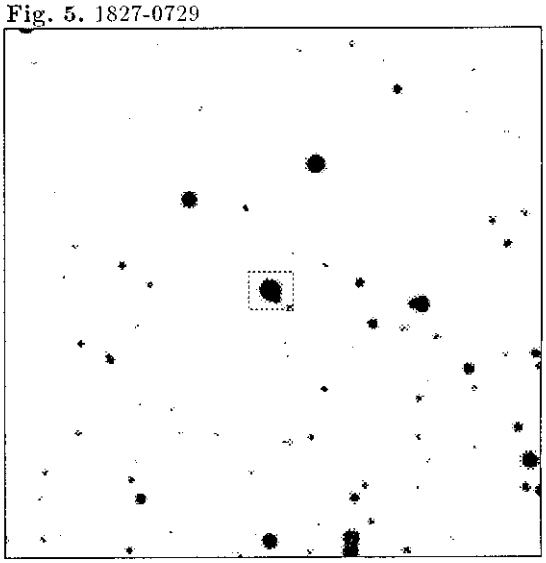

Fig. 6. 1839-1418

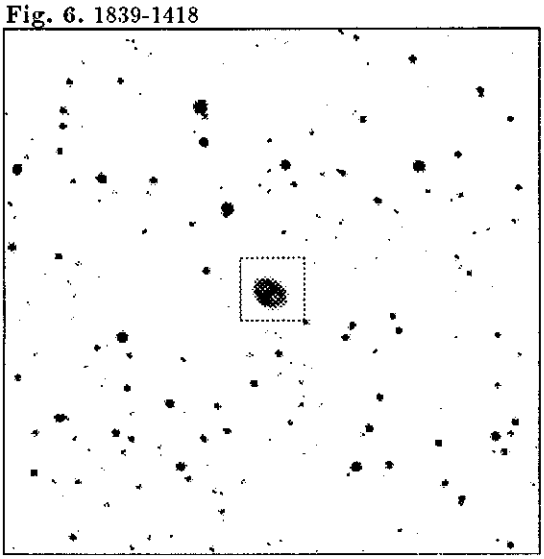

Fig. 7. 1840-1109

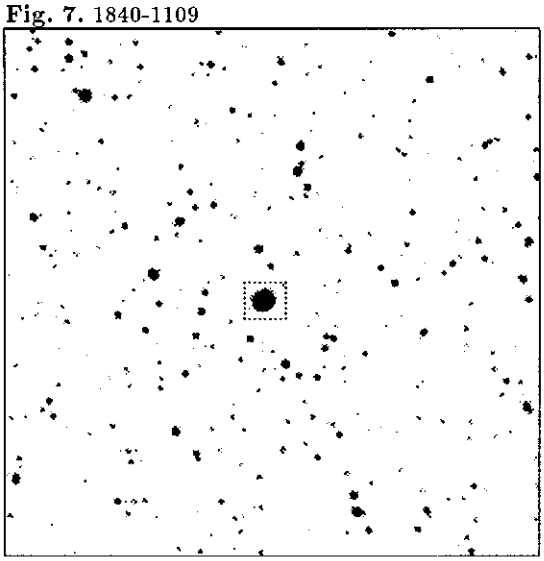

Fig. 8. 1841+0343

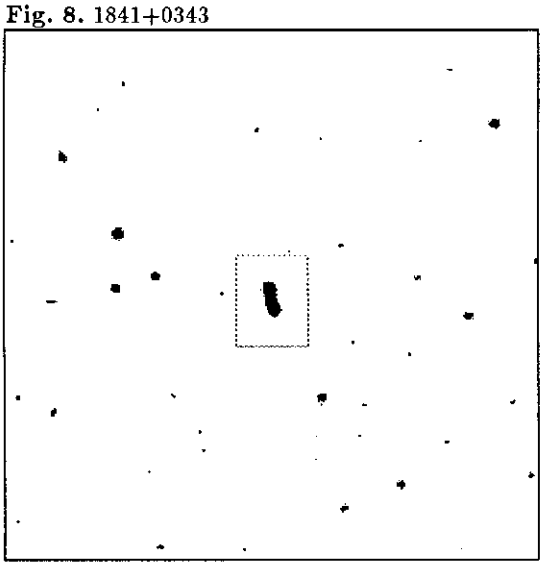

Fig. 9. 1858+0821

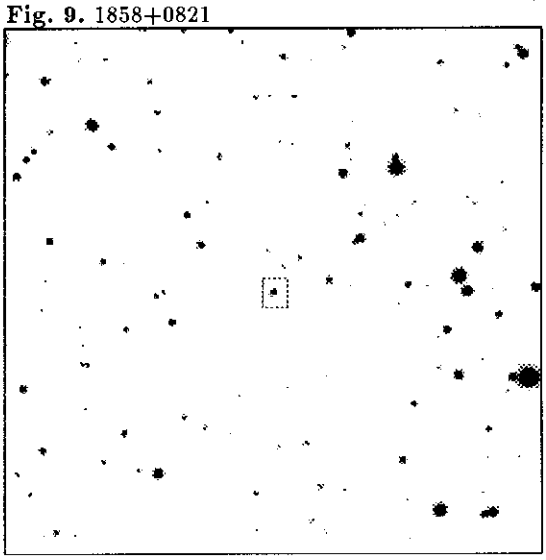

Fig. 10. 1859+1013

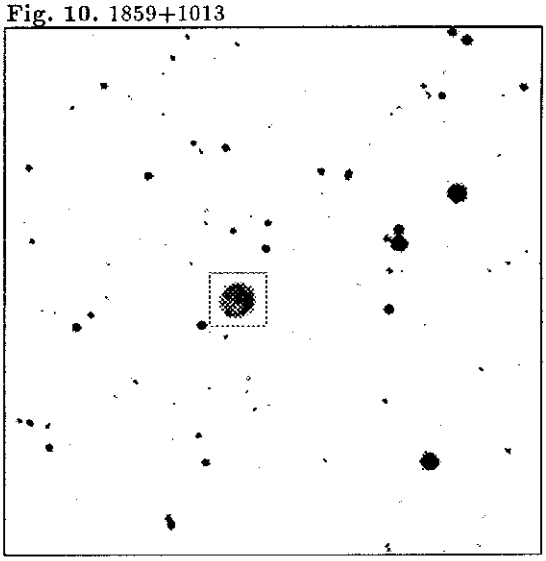

Fig. 11. 1904+1038

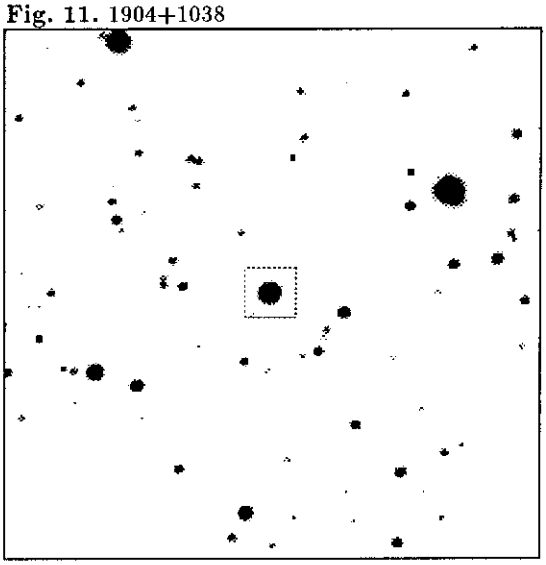

Fig. 12. 1908+0422

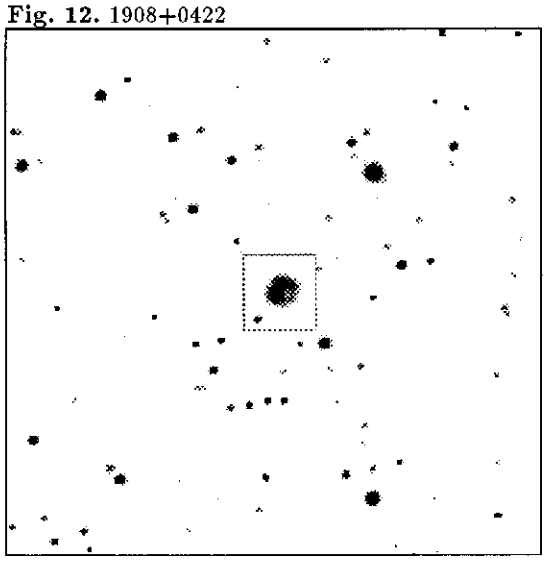

Fig. 13. 1909+1326

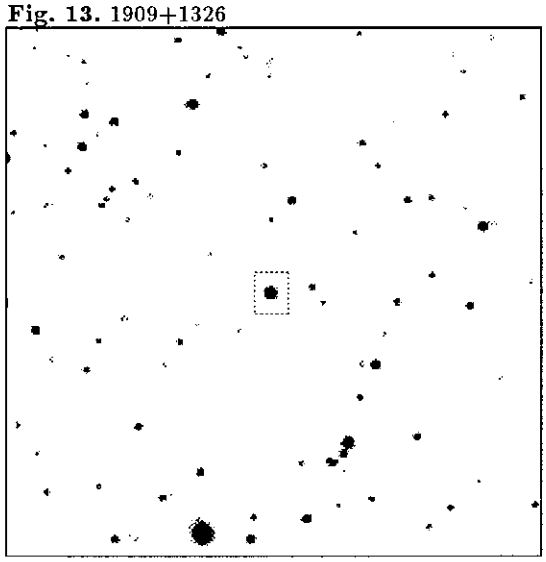

Fig. 14. 1911+1534

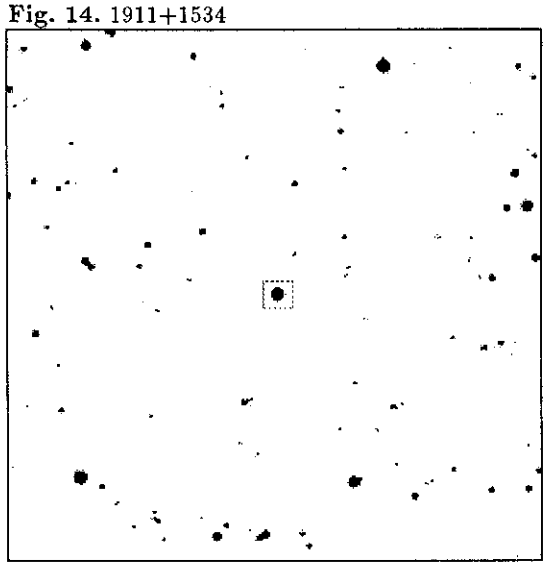

Fig. 15. 1920+1122

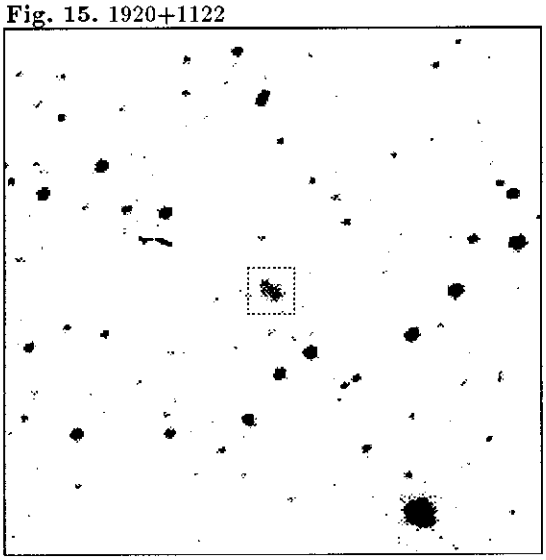

Fig. 16. 1933-0400

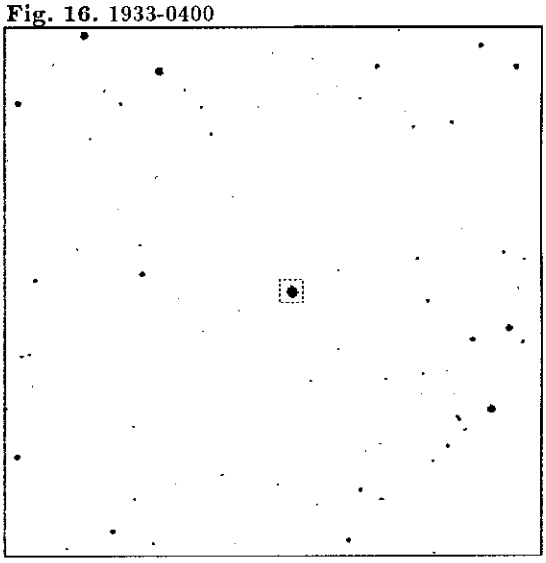

Fig. 17. 1943+2251

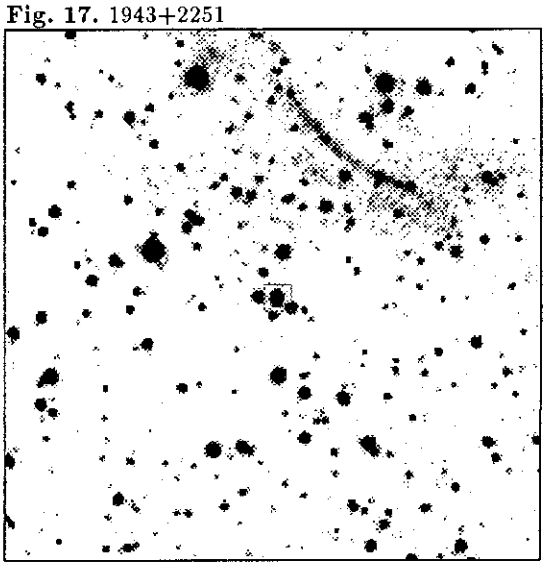

B. Contour plots

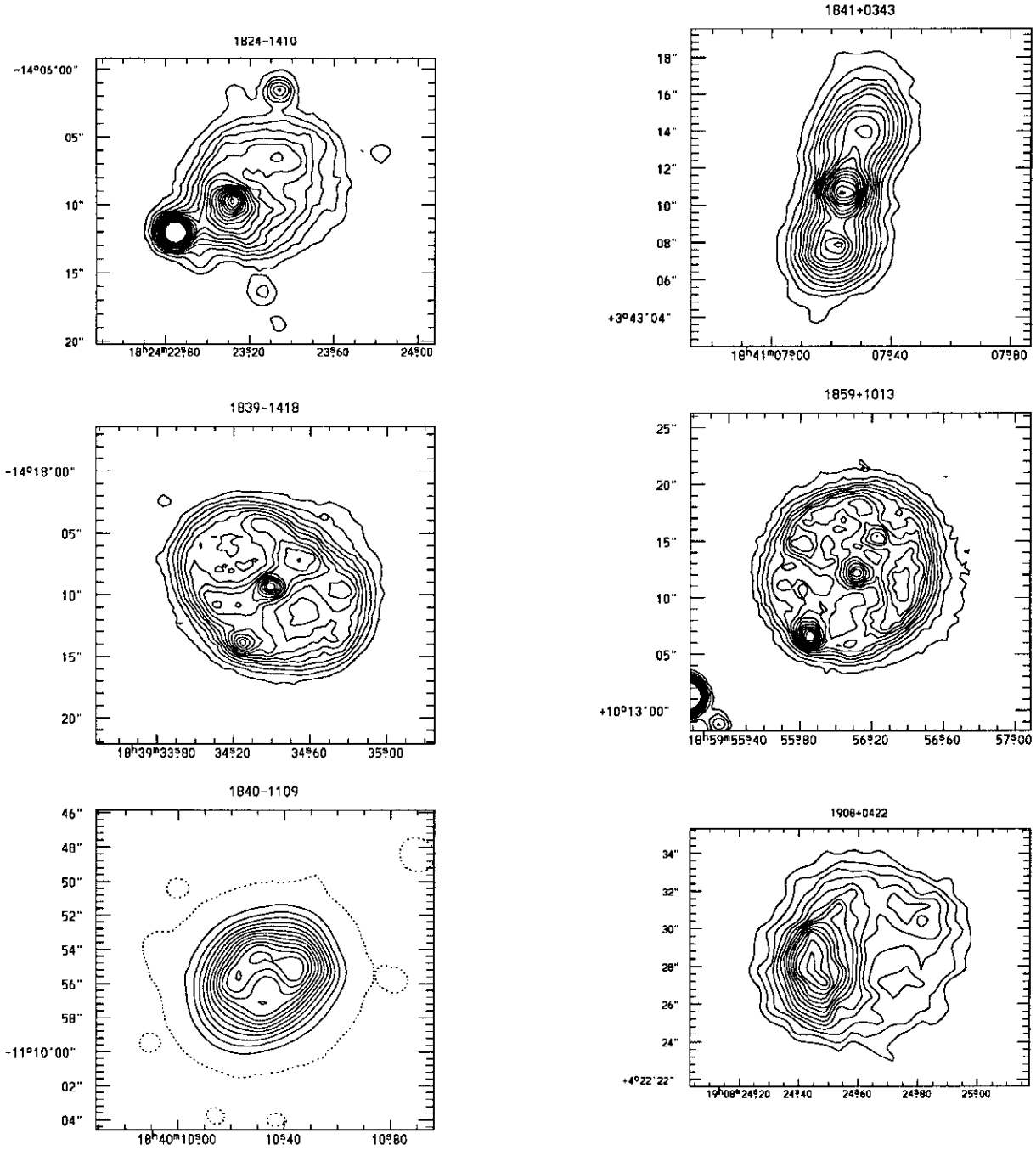

Top left: the outer, lowest contour is at 15% of the peak; the stepsize is 5% of the peak.
Middle left: the outer, lowest contour is at 25% of the peak; the stepsize is 5% of the peak
Bottom left: the outer, lowest contour is at 2% of the peak; the stepsize is 8% of the peak.
Top right: the outer, lowest contour is at 15% of the peak; the stepsize is 5% of the peak.
Middle right: the outer, lowest contour is at 35% of the peak; the stepsize is 5% of the peak
Bottom right: the outer, lowest contour is at 30% of the peak; the stepsize is 5% of the peak.

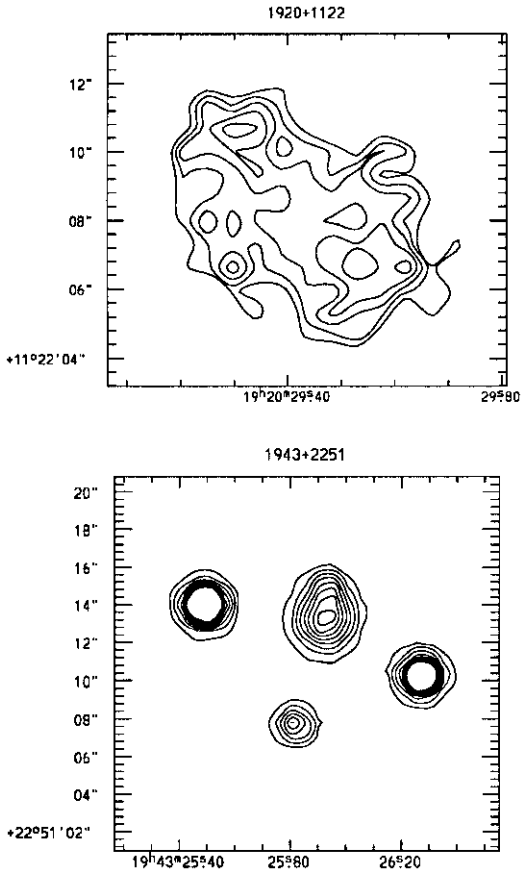

Top: the outer, lowest contour is at 75% of the peak; the stepsize is 5% of the peak.
Bottom: the outer, lowest contour is at 25% of the peak; the stepsize is 10% of the peak.

C. Optical spectra

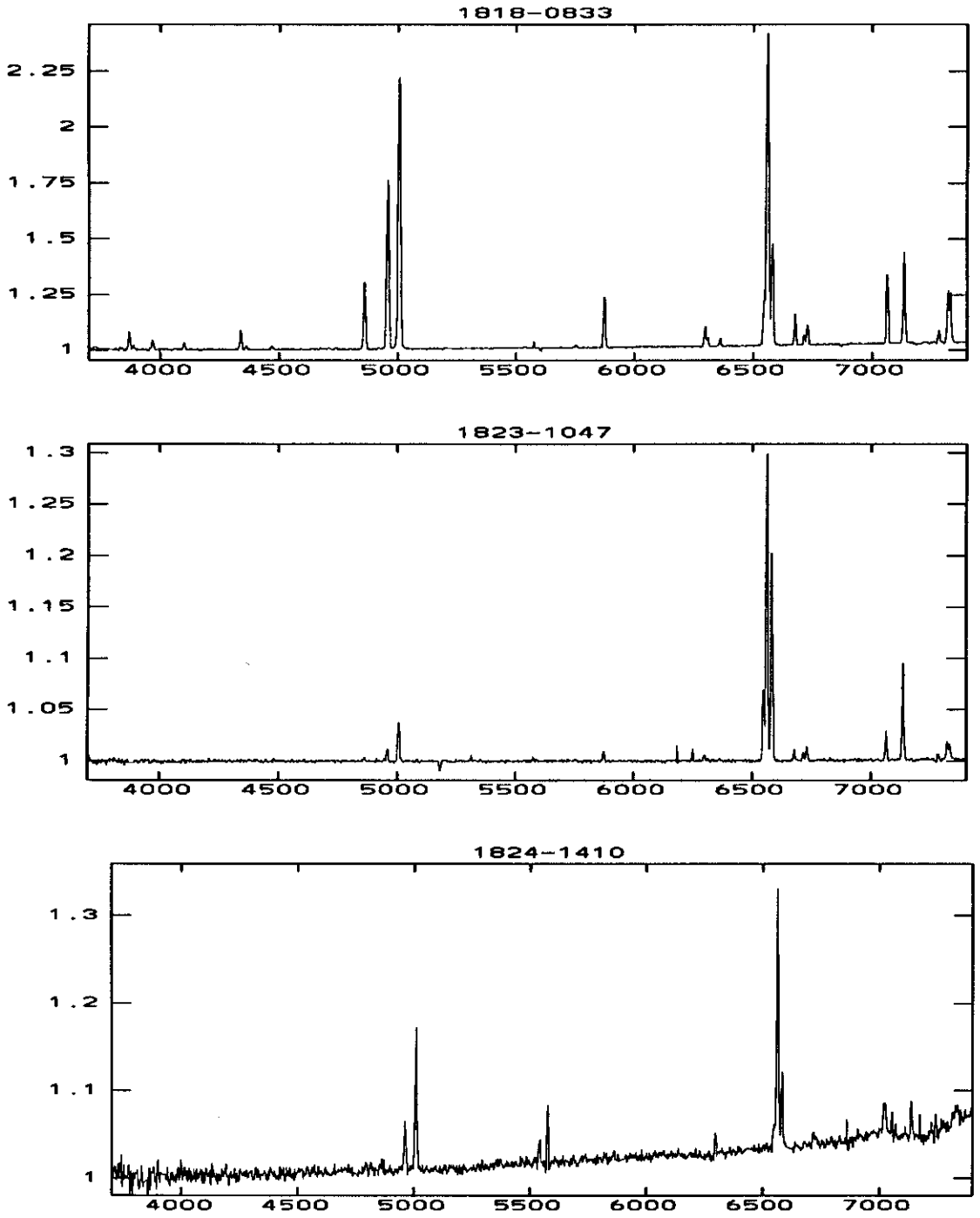

Spectra of IRAS-selected planetary nebulae. Above every spectrum the object is mentioned.
X**-axis**: wavelength from 3.700 Å to 7.400 Å
Y**-axis**: Log$(10 + I\ 10^{15})$ in ergs/cm^2/s/Å.

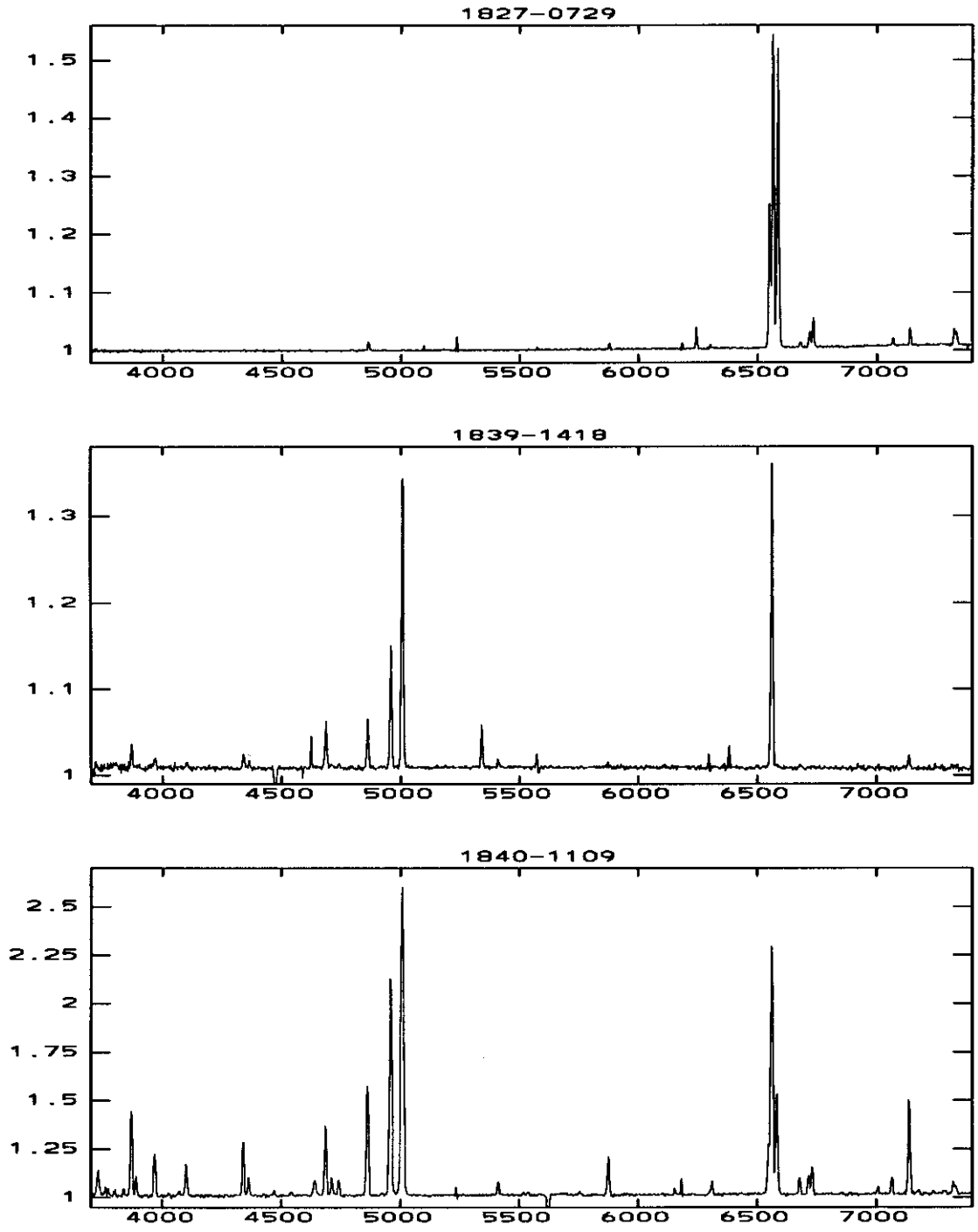

Spectra of IRAS-selected planetary nebulae. Above every spectrum the object is mentioned.
X**-axis**: wavelength from 3.700 Å to 7.400 Å
Y**-axis**: Log(10 + I 10^{15}) in ergs/cm^2/s/Å.

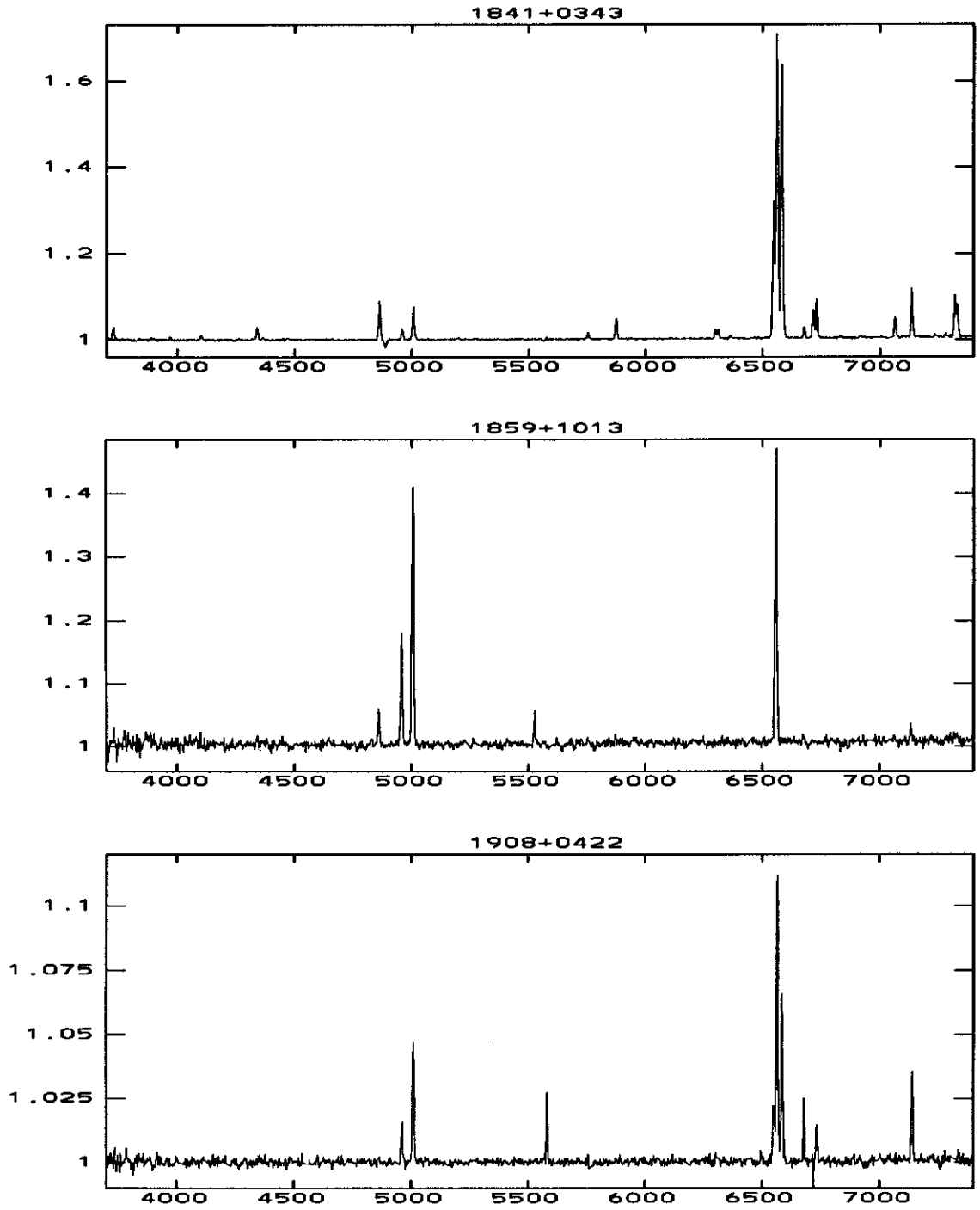

Spectra of IRAS-selected planetary nebulae. Above every spectrum the object is mentioned.
X**-axis**: wavelength from 3.700 Å to 7.400 Å
Y**-axis**: Log(10 + I 10^{15}) in ergs/cm^2/s/Å.

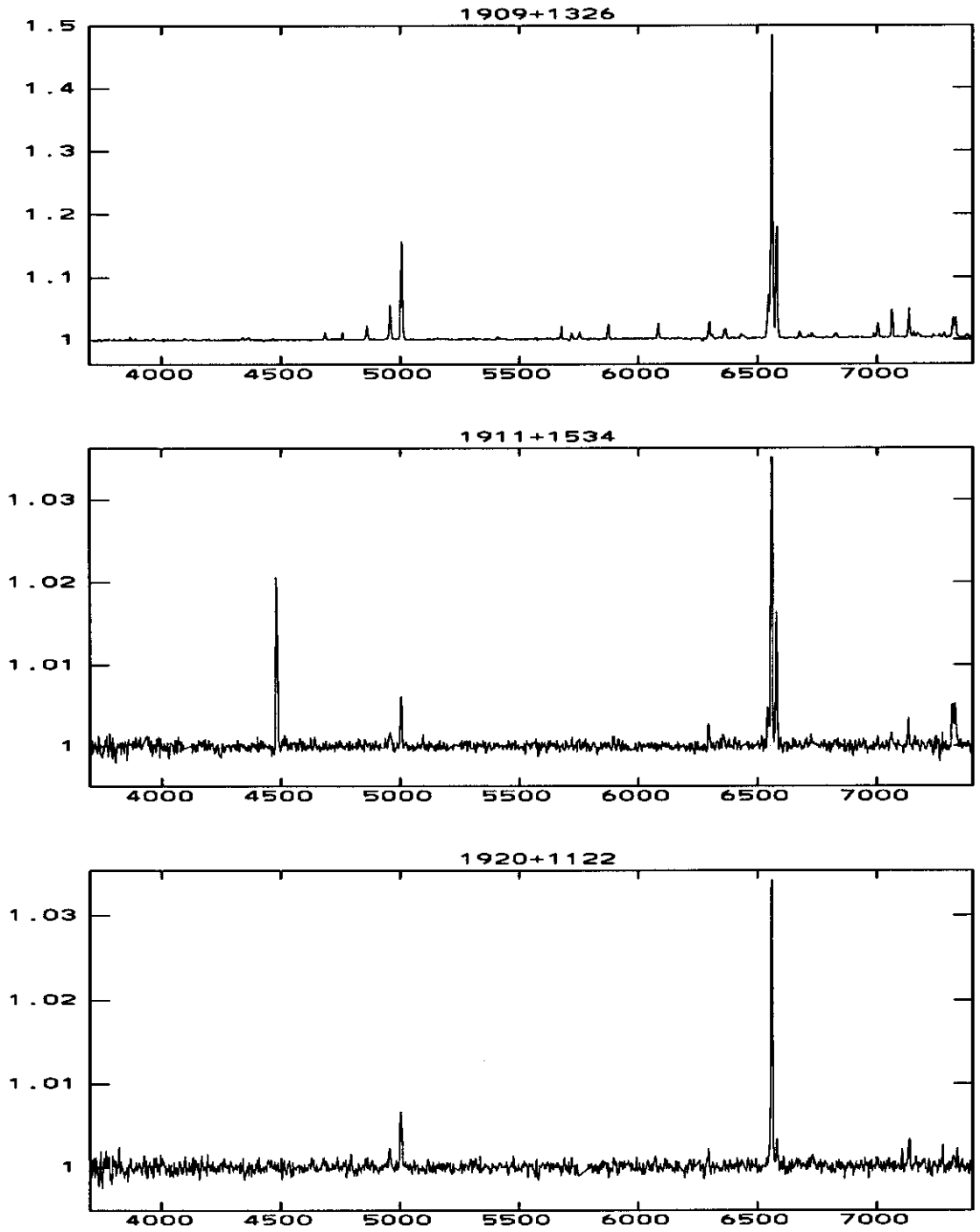

Spectra of IRAS-selected planetary nebulae. Above every spectrum the object is mentioned.
X**-axis**: wavelength from 3.700 Å to 7.400 Å
Y**-axis**: Log(10 + I 10^{15}) in ergs/cm^2/s/Å.

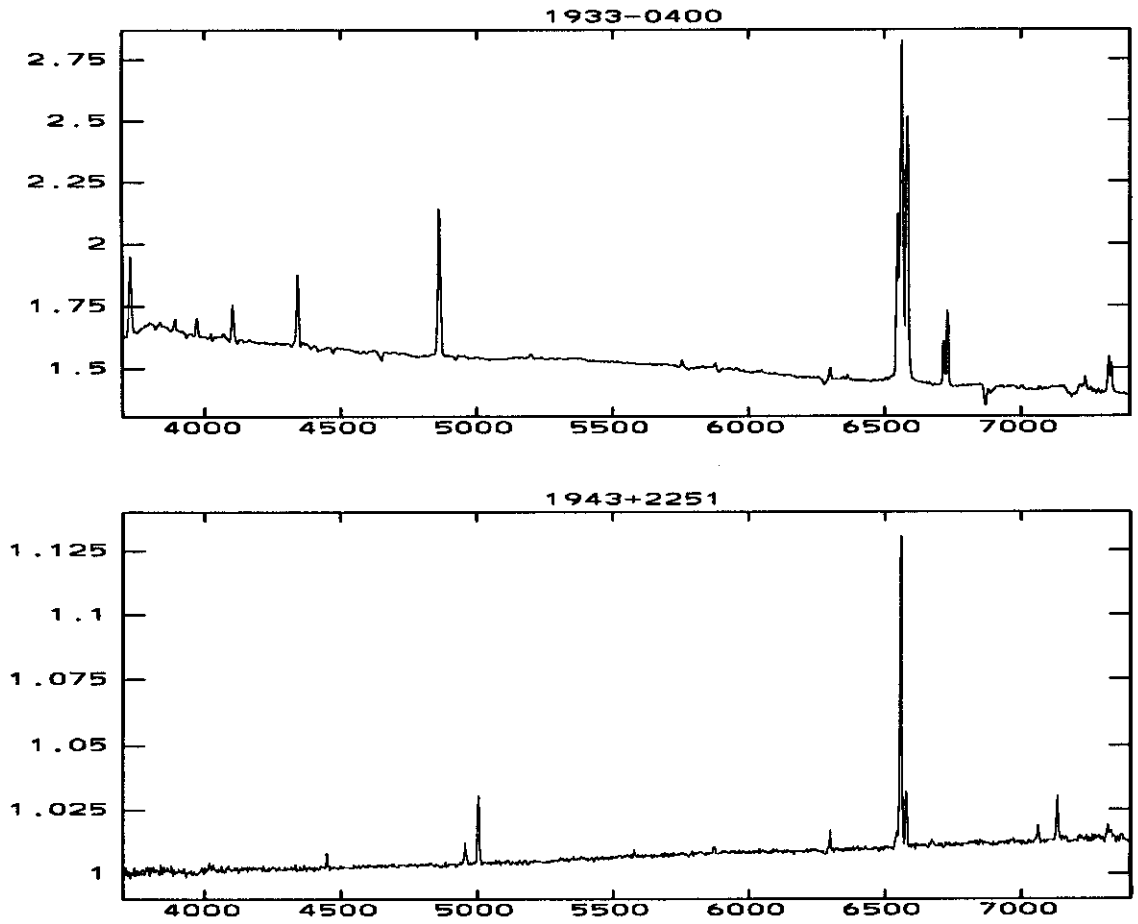

Spectra of IRAS-selected planetary nebulae. Above every spectrum the object is mentioned.
X**-axis**: wavelength from 3.700 Å to 7.400 Å
Y**-axis**: Log$(10 + I\ 10^{15})$ in ergs/cm^2/s/Å.

D. Line flux ratios

Line fluxes corrected for interstellar extinction relative to Hβ or [O III]λ5007.
An estimate of the percentual uncertainty in the relative flux (err) is also given.
Contaminated lines are indicated by a colon.

λ(Å)	Ident	1818–0833		1823–1047		1824–1410		1827–0729		1839–1418		1840-1109		1841+0343	
		Flux	err	Flux	err	Flux	err	Flux	err	Flux	err	Flux	err	Flux	err
3727	[O II]											28.3	10	138.6	10
3750	H I														
3771	H I											3.1	15		
3798	H I														
3835	H I											4.9	10		
3869	[Ne III]	88.0	10							92.9	10	110.3	10		
3889	He I, H I	21.1	12									16.6	10	5.9	57
4026	He I	1.9	46									1.1:	36		
4069	[S II]											1.4	28		
4076	[S II]														
4102	H I	20.2	10							22.0	19	25.9	10	20.8	13
4340	H I	47.4	10							50.7	10	45.9	10	56.1	10
4363	[O III]	7.0	10							19.7	16	11.7	10		
4471	He I	6.8	17									2.6	13		
4686	He II									99.1	10	53.3	10		
4740	[Ar IV]	2.1	16							4.9	43	7.5	10		
4861	H I	100.0	10	11.1	28	8.9	18	100.0	10	100.0	10	100.0	10	100.0	10
4959	[O III]	403.0	10	31.8	10	36.6	10			251.1	10	423.1	10	21.9	10
5007	[O III]	1217	10	100.0	10	100.0	10	10.0	50	754.1	10	1266	10	69.6	10
5309	[Ca V]			3.7	20										
5518	[Cl III]											1.3	22		
5538	[Cl III]	0.6	21									1.7	35		
5577	[O I]			0.8	51	11.3	10			7.6	15			1.4:	30
5755	[N II]	0.8	13	0.5	49			1.4	50			0.5:	25	3.1	10
5876	He I	16.5	10	1.9	10			7.2	10			11.6	10	15.4	10
6300	[O I]	3.4	10	0.5	15	1.8	11	1.4	16	4.3	17	0.7	22	4.6	10
6312	[S III]	1.3	10					0.6	43			3.1	10	4.3	10
6364	[O I]	1.1	10	0.1	53									0.5:	41
6435	[Ar V]														
6548	[N II]	8.4	10	5.7	10	2.7	26	89.3	10			13.0	10	78.0	10
6563	H I	285.0	10	31.8	10	25.2	10	285.0	10	285.0	10	285.0	10	285.0	10
6583	[N II]	19.8	10	17.6	10	4.9	10	270.1	10			36.3	10	245.1	10
6678	He I	4.0	10	0.5	10			1.8	10			3.4	10	4.0	10
6716	[S II]	1.3	10	0.5	10	1.4	22	6.2	10			3.6	10	10.0	10
6731	[S II]	2.5	10	0.9	10			11.2	10			5.6	10	14.7	10
7006	[Ar V]											1.1	10		10
7065	He I	8.9	10	1.0	10			1.5	10			3.4	10	4.8	10
7136	[Ar III]	12.3	10	3.3	10	1.8	10	1.8	10	7.5	10	27.4	10	14.0	10
7281	He I	1.0	10	0.1	13			0.5	18			0.4	21	0.4	33
7320	[O II]	4.6	10	0.4	10	1.2	24	3.1	10	2.1	20	1.9	10	10.3	10
7331	[O II],[Ar IV]	4.7	10	0.3	10	0.8	12	2.9	10	2.3	24	1.6	10	8.9	10

Line fluxes corrected for interstellar extinction relative to Hβ or [O III]λ5007.
An estimate of the percentual uncertainty in the relative flux (err) is also given.
Contaminated lines are indicated by a colon.

λ(Å)	Ident	1859+1013		1908+0422		1909+1326		1911+1534		1920+1122		1933-0400		1943+2251	
		Flux	err	Flux	err	Flux	err	Flux	err	Flux	err	Flux	err	Flux	err
3727	[O II]											69.3	10		
3750	H I														
3771	H I														
3798	H I														
3835	H I											1.5	10		
3869	[Ne III]					1.6	40								
3889	He I, H I					5.7	75					5.5	10		
4026	He I														
4069	[S II]											1.8	10		
4076	[S II]														
4102	H I											22.4	10		
4340	H I					35.2	11					45.2	10		
4363	[O III]					42.4	11								
4471	He I					2.5	90								
4686	He II					61.2	10								
4740	[Ar IV]					3.6	57								
4861	H I	100.0	10			100.0	10					100.0	10		
4959	[O III]	293.6	10	24.1	10	203.4	10	12.1	51	30.5	23			34.8	10
5007	[O III]	884.4	10	100.0	10	604.9	10	100.0	10	100.0	10			100.0	10
5309	[Ca V]														
5518	[Cl III]														
5538	[Cl III]														
5577	[O I]													1.7	24
5755	[N II]	7.0	48			11.2	10					1.3	10		
5876	He I	5.7	34			15.5	10					0.7	10	1.5	25
6300	[O I]					12.6	10	4.9	13			1.7	10	1.3	10
6312	[S III]					2.9	10								
6364	[O I]					4.3	10								
6435	[Ar V]					3.8	26								
6548	[N II]			2.5	10	27.3	10	7.2	10			45.8	10	1.4	10
6563	H I	285.0	10	16.1	10	285.0	10	50.4	10	33.9	1	285.0	10	26.5	10
6583	[N II]			8.0	10	69.8	10	21.2	10	1.8	19	137.4	10	3.9	10
6678	He I					3.3	10							0.4	25
6716	[S II]			1.5	10	1.1	11					5.7	10		
6731	[S II]			1.6	10							11.2	10		
7006	[Ar V]					4.9	10								
7065	He I	2.1	43			9.1	10							0.7	10
7136	[Ar III]	6.0	17	2.1	10			2.4	11	1.6	15			1.6	10
7281	He I					1.1	10								
7320	[O II]					5.4	10	2.4	10			3.5	10	0.2	15
7331	[O II], [Ar IV]					5.2	10	3.2	10			3.1	10	0.2	45